A probabilistic approach to characterizing drought using satellite gravimetry

Peyman Saemian[1], Mohammad J. Tourian[1], Omid Elmi[1]

Nico Sneeuw[1], Amir AghaKouchak[2,3]

[1]Institute of Geodesy, University of Stuttgart, Stuttgart, Germany

[2]Department of Civil and Environmental Engineering, University of California, Irvine, CA, USA.

[3]United Nations University Institute for Water, Environment and Health, Hamilton, Ontario, Canada

Key Points:

- A probabilistic framework is introduced to characterize drought using GRACE and GRACE Follow-On observations.
- Our study highlights a tendency of deterministic approaches to consistently overestimate storage-based drought severity.
- The probabilistic approach captures global droughts while delivering more realistic results suited for risk management.

Corresponding author: Peyman Saemian, `peyman.saemian@gis.uni-stuttgart.de`

Abstract

In the recent past, the Gravity Recovery and Climate Experiment (GRACE) satellite mission and its successor GRACE Follow-On (GRACE-FO), have become invaluable tools for characterizing drought through measurements of Total Water Storage Anomaly (TWSA). However, the existing approaches have often overlooked the uncertainties in TWSA that stem from GRACE orbit configuration, background models, and intrinsic data errors. Here we introduce a fresh view on this problem which incorporates the uncertainties in the data: the Probabilistic Storage-based Drought Index (PSDI). Our method leverages Monte Carlo simulations to yield realistic realizations for the stochastic process of the TWSA time series. These realizations depict a range of plausible drought scenarios that later on are used to characterize drought. This approach provides probability for each drought category instead of selecting a single final category at each epoch. We have compared PSDI with the deterministic approach (SDI) over major global basins. Our results show that the deterministic approach often leans towards an overestimation of storage-based drought severity. Furthermore, we scrutinize the performance of PSDI across diverse hydrologic events, spanning continents from the United States to Europe, the Middle East, Southern Africa, South America, and Australia. In each case, PSDI emerges as a reliable indicator for characterizing drought conditions, providing a more comprehensive perspective than traditional deterministic indices. In contrast to the common deterministic view, our probabilistic approach provides a more realistic characterization of the TWS drought, making it more suited for adaptive strategies and realistic risk management.

Plain Language Summary

Total Water Storage (TWS) is defined as the sum of water stored as surface water (e.g., lakes and rivers), groundwater, soil moisture, snow, ice, and vegetation biomass. Since its launch in 2002, the Gravity Recovery and Climate Experiment (GRACE) satellite mission has provided unique TWS change measurements with manifold applications in hydrology,

including characterizing drought events. Scientists have been using satellites like GRACE and its successor, GRACE-FO, to understand drought by measuring the Total Water Storage Anomaly (TWSA). However, previous methods didn't consider uncertainties from satellite orbits, models, and data errors. This study offers a novel probabilistic approach for characterizing drought, Probabilistic Storage-based Drought Index (PSDI), which acknowledges the uncertainties in the GRACE TWS change. We use simulations to create different drought scenarios, offering probabilities for each category instead of one fixed category. Comparing PSDI to traditional methods, we found that traditional methods tend to overestimate drought severity. We tested PSDI across different regions, and it consistently proved to be a reliable way to understand drought conditions, offering a more comprehensive perspective. Our probabilistic approach offers a more realistic view of TWS drought, making it suitable for adaptive strategies and risk management.

1 Introduction

The modern reality of human settlement is the consequence of many historical events, but perhaps none influenced human settlements as much as droughts and famine. DNA analysis indicates that a series of extreme droughts that occurred 75-135 thousand years ago may have been the reason for the first human migration out of Africa (Scholz et al., 2007). Following several consequential droughts over the past century (e.g., the 1921 drought in Europe, the 1930s Dust Bowl drought in the US, 1928-1930 drought in China, 1980s drought and famine in Africa, 2000s Millennium drought in Australia), increasingly more effort has focused on understanding, monitoring and predicting droughts and their impacts (Mishra & Singh, 2010; Heim Jr, 2002; AghaKouchak et al., 2015; Svoboda et al., 2002; Wilhite et al., 2007; Kreibich et al., 2022; AghaKouchak et al., 2021).

Compared to other hazards witnessed over the past four decades, drought impacts are often felt by a much larger number of people worldwide (Wilhite, 2000; FAO, 2021; AghaKouchak et al., 2021). Numerous nations have grappled with significant economic losses resulting

from drought events. Notably, according to the NOAA's National Centers for Environmental Information (NCEI) report, the United States has experienced 26 significant droughts in the past century, amounting to a staggering economic loss of at least $ 249 billion, equivalent to nearly $ 10 billion per occurrence. In Europe, the southern and western regions, in particular, face an annual drought-related expenditure estimated at up to € 9 billion, which could surge to over € 65 billion if climate action is not taken (Naumann et al., 2021). Aside from the financial burdens, climate change, and unsustainable water management practices have amplified the frequency and severity of drought occurrences worldwide over the past two decades. This trend is projected to escalate further in the future (see e.g., Hisdal et al., 2001; Coumou & Rahmstorf, 2012; Yu et al., 2014; Donat et al., 2016; Teuling, 2018; Li et al., 2021; C. Zhao et al., 2020).

The negative consequences of drought can be effectively alleviated through the implementation of risk management strategies rather than relying on crisis management (Wilhite, 2000; Zscheischler et al., 2018). Such a proactive response may be achieved by establishing reliable drought monitoring systems, including early warning systems and forecasting capabilities, operating at both national and local levels (Wilhite et al., 2007; AghaKouchak et al., 2023). These systems trigger a series of decisions aimed at helping communities navigate the challenges posed by drought events (Mishra & Singh, 2011; Sun et al., 2017). To enhance drought monitoring efforts and provide valuable guidance to decision-makers, numerous drought indices have been developed (Mishra & Singh, 2010). These indices condense the intricacies of drought into a single numerical value, effectively characterizing its onset, intensity, frequency, and duration (Zargar et al., 2011; Wilhite, 2000; Ahmadalipour et al., 2017). Such indices offer a comprehensive representation of drought by utilizing single or multiple climatic and hydrometeorological variables such as precipitation, streamflow, evapotranspiration, temperature, and snowpack (e.g., Svoboda et al., 2016; Hosseini-Moghari et al., 2020).

A comprehensive understanding of drought dynamics necessitates the observation of Total Water Storage (TWS) including snow, surface water, soil moisture, and groundwater storage (M. Zhao et al., 2017; M. J. Tourian et al., 2023). Traditionally, TWS monitoring has relied on costly and time-consuming site measurements, providing limited regional and local coverage. While hydrological and land surface models partially address this issue, estimating TWS in regions lacking in-situ runoff data for calibrating rainfall-runoff models still yields high uncertainties (Jiang et al., 2014; S. Yi et al., 2023). Since its launch in 2002, the Gravity Recovery And Climate Experiment (GRACE) satellite mission has revolutionized the remote measurement of TWS Anomalies (TWSA) at regional to continental scales (Tapley et al., 2004; M. J. Tourian et al., 2022). The GRACE mission came to an end on 12 October 2017, due to battery failure, after more than 15 years of Earth observation. However, its successor, GRACE Follow-On (GRACE-FO), has continued the GRACE legacy since its launch on 22 May 2018. GRACE(-FO) data have been extensively utilized for manifold applications, including monitoring ice sheets and glaciers (e.g., van den Broeke et al., 2009; Gardner et al., 2013; Shepherd et al., 2018), tracking anthropogenic groundwater depletion (e.g., Rodell et al., 2007, 2009; Famiglietti et al., 2011; Voss et al., 2013; Saemian et al., 2022), forecasting flood events (e.g., Reager & Famiglietti, 2009; Gouweleeuw et al., 2018), and quantifying and comprehending hydrological processes (e.g., Lorenz et al., 2014; Saemian et al., 2020; M. Tourian et al., 2018; Behling et al., 2022), to name but a few.

GRACE-derived estimates of TWS have been employed in developing indices aimed at assessing drought on a regional to global scale. For example, Yirdaw et al. (2008) developed the Total Storage Deficit Index (TSDI), utilizing the Palmer Drought Severity Index (PDSI; Palmer, 1965) and the Soil Moisture Deficit Index (SMDI; Narasimhan & Srinivasan, 2005), to characterize the Canadian Prairie droughts of 2002/2003. Another notable endeavor by Thomas et al. (2014) presented a comprehensive framework for drought characterization based on GRACE-derived TWSA over regions including the Amazon, Zambezi, Texas, and the southeastern United States. Additionally, H. Yi & Wen (2016) devised the GRACE-based Hydrological Drought Index (GHDI) to characterize drought in the continental United

States from 2003 to 2012, building upon the foundation of the PDSI concept. Among recent indicators we can name the Drought Severity Index (DSI) by M. Zhao et al. (2017), the Water Storage Deficit Index (WSDI) by Sinha et al. (2017), and a long-term standardized GRACE reconstructed TWSA index (SGRTI) by Zhong et al. (2023).

The indices mentioned above have the potential for monitoring and assessing the TWS drought at regional to global scales. Nevertheless, they adopt a deterministic approach that disregards the intrinsic uncertainties associated with characterizing drought using GRACE observations. These uncertainties are inherent in the GRACE data due to factors such as its orbit configuration, measurement concept, various post-processing approaches of GRACE data, and different options for de-aliasing products. Besides, the estimation of GRACE uncertainty varies among different GRACE level-2 products, in both magnitude and spatial pattern. Most of the centers offer an uncertainty measure (known as formal errors) in the form of spherical harmonic coefficients. Figure 1 shows the coefficient-wise ratio of average formal errors and empirical errors of the GRACE solution following the approach suggested by Kvas et al. (2019). The ideal ratio is set at one, with values below indicating an underestimation of empirical errors, whereas values exceeding one signify an overestimation. The three official centers (JPL, CSR, and GFZ) together with AIUB, HUST, and SWPU exhibit a similar pattern. The SWPU solution demonstrates a pronounced overestimation of formal errors, particularly for low d/o (under 30). ITSG and Tongji display comparable patterns, although Tongji tends to lean slightly towards a more pessimistic estimation of errors. In contrast, COST-G reflects more realistic formal errors in comparison to empirical errors but appears overly optimistic for lower d/o values. The distinctive pattern observed in the CNES product can be attributed to the regularization applied during the derivation of the gravity field from the Level-1 dataset. The disparities in formal error performance among GRACE Level-2 products underscore the inherent uncertainty in GRACE data and consequently, the necessity for a comprehensive approach that effectively considers GRACE uncertainty while characterizing drought.

To address this gap in conventional methods, we propose a probabilistic approach that considers all possible scenarios and associated impacts. Our approach leverages Monte Carlo simulations to obtain realistic realizations of TWSA compatible with GRACE-TWSA and its corresponding uncertainties. We then characterize drought based on TWSA using our proposed drought index, the Probabilistic Storage-based Drought Index (PSDI). This index indicates not only drought but also its corresponding occurrence probability. We compare our results with those from the conventional deterministic approaches over the major river basins. Moreover, the performance of PSDI in capturing the main hydrological drought extremes is examined within the GRACE era. PSDI facilitates more informed and proactive responses to water resource challenges and serves as a practical tool for decision-makers and water resource managers to assess and manage drought-related risks more realistically.
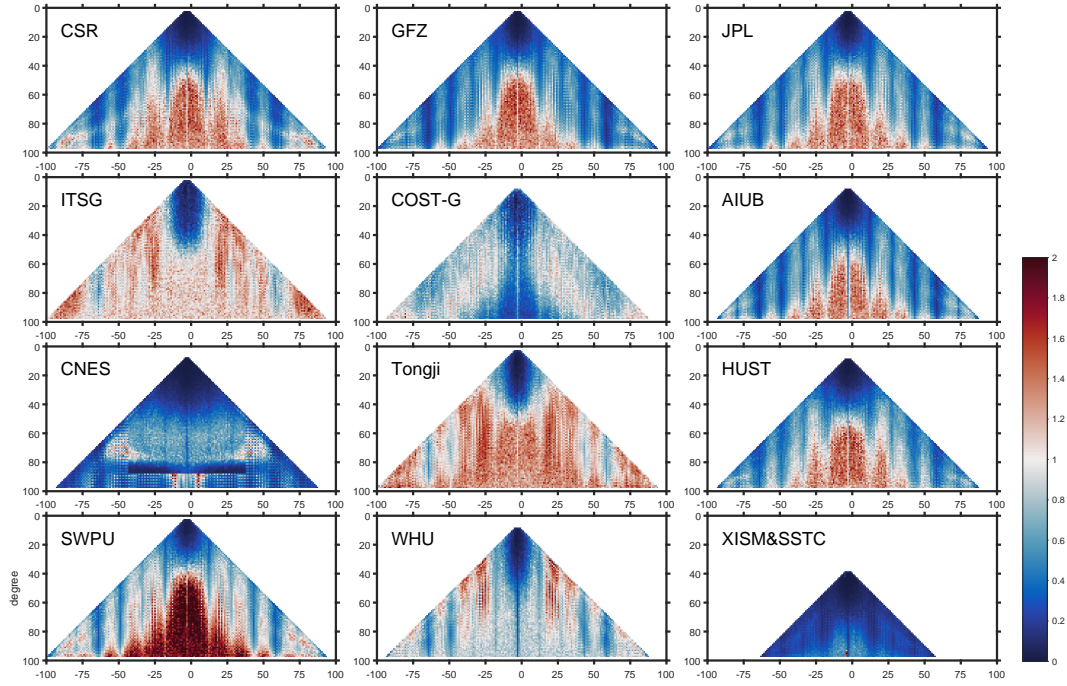

Figure 1. The coefficient-wise ratio of average formal errors and empirical errors of the GRACE solutions following the approach suggested by Kvas et al. (2019). For the average formal errors, the mean of the reported variance of the spherical harmonics coefficients is computed for monthly solutions from January 2005 to December 2010, which is assumed to hold a homogeneous data quality. To estimate the empirical errors, we compute the standard deviation of the coefficients after removing the mean, linear trend, and annual and semi-annual signals. The optimal value of the ratio is one, and values below one indicate an underestimation of the empirical errors, while values bigger than one show overestimation. We have only included solutions that provide formal errors.

2 Data and Method

2.1 GRACE data

The GRACE TWSA can be obtained from the two main approaches, namely Spherical Harmonics (SHs) and mass concentration blocks (mascons). In the former, one needs to apply post-processing steps including noise reduction and signal restoration while the latter is already the Level-3 product (gridded TWSA over the globe). These approaches are briefly described in section 1 of the supplementary file. In line with the common practice within the hydrology community, we have utilized the mascons solutions. The probabilistic approach for characterizing storage-based drought index, however, can readily be applied to any level-3 products that provide estimations for GRACE TWSA and its corresponding uncertainty. Among the mascon products, we have employed the one from Goddard Space Flight Center (GSFC), NASA. The GSFC mascon product has been widely used in the geodesy and Earth science communities to investigate a range of phenomena, including hydrology, glaciology, and solid Earth dynamics, and can be downloaded from `https://earth.gsfc.nasa.gov/geo/data/grace-mascons`. We used the latest version of the dataset available at the time of our analysis, which covers the period from August 2002 to November 2022. The dataset includes monthly gravity field solutions with a grid size of $0.5\,°$.

2.2 Methodology

We propose a probabilistic framework to characterize storage-based drought. The framework is illustrated in Figure 2, Figure 3, and Figure 4 using TWSA over the Death Valley basin in the US as an example. To characterize drought, we must first define a reference, based on which a prolonged relative water deficiency is determined. It is common to consider the long-term monthly average, also known as the *climatology*, as the reference or *normal* condition in a region. Obtaining accurate climatology from short time series can be challenging. Calculating the climatology over at least 30 years, preferably 60 years, is standard practice, as this time frame allows us to average out the effects of short-term variability, resulting

₁₈₅ in a more robust estimate of the long-term average conditions (e.g., Hulme, 1992; Jones &

₁₈₆ Hulme, 1996; Svoboda et al., 2012). The GRACE and GRACE-FO missions, with their

₁₈₇ approximately 20-year duration, fall short of providing sufficient data for calculating long-

₁₈₈ term climatology. In this study, we utilized a combination of different models to estimate

₁₈₉ TWSA dating back to 1980. To this end, we incorporated a total of 13 state-of-the-art

₁₉₀ datasets including Global Hydrological Models (GHMs), Land Surface Models (LSMs), and

₁₉₁ atmospheric reanalysis models. To combine models, we employed the Multivariate Linear

₁₉₂ Regression (MLR) method. We compared the results of Multiple Linear Regression (MLR)

₁₉₃ in reconstructing TWSA with GRACE time series (see Supplementary section 2). The MLR

₁₉₄ exhibits a strong capability to capture the features and effectively reconstruct TWSA data

₁₉₅ as far back as 1980. It demonstrated superior performance compared to the ensemble mean

₁₉₆ of the models, as indicated by a substantial improvement in both the correlation coefficient

₁₉₇ (on average from 0.87 to 0.97) and the Kling-Gupta Efficiency (KGE) score (on average from

₁₉₈ 0.27 to 0.95) across major river basins. For more details about the datasets and long-term

₁₉₉ TWSA, please refer to Supplementary section 2. This extended time frame enables us to

₂₀₀ capture significant climate events and phenomena that influence long-term climate, such as

₂₀₁ the El Niño-Southern Oscillation (ENSO) and the North Atlantic Oscillation (NAO) (Sohn

₂₀₂ et al., 2013; Coelho & Goddard, 2009).

₂₀₃ The climatology, along with its corresponding uncertainty (see Figure 2 (a)), is obtained by:

$$\overline{\mathrm{TWSA}}[t_m] = \frac{1}{N} \sum_{y=y_1}^{y_N} \mathrm{TWSA}[t_{y,m}] \tag{1}$$

$$\sigma_{\overline{\mathrm{TWSA}}[t_m]}^2 = \frac{1}{N} \sqrt{\sum_{y=y_1}^{y_N} \sigma_{\mathrm{TWSA}[t_{y,m}]}^2} \tag{2}$$

₂₀₄ where $\overline{\mathrm{TWSA}}[t_m]$ represents the TWSA climatology for month m, y denotes the year and can

₂₀₅ vary from y_1 to y_N, m corresponds to the month within a year, taking values $1, 2, 3, \ldots, 12$,

206   and N is the number of years in the long-term dataset. Note that we deliberately retain

207   the trend in the time series. We reason that the trend reflects long-term changes in climate,

208   such as temperature increases or precipitation pattern alterations, and that it affects the

209   frequency and severity of droughts (see Supplementary section 3 for more details). We then

210   subtract the climatology from the GRACE TWSA time series to obtain TWS residual (S):

$$S[t_{y,m}] = \text{TWSA}[t_{y,m}] - \overline{\text{TWSA}}[t_m] \tag{3}$$

$$\sigma_{S[t_{y,m}]} = \sqrt{\sigma^2_{\text{TWSA}[t_{y,m}]} + \sigma^2_{\overline{\text{TWSA}}[t_m]}} \tag{4}$$

211   where negative values of S represent water storage deficits.

212   To reduce the effects of short-term fluctuations due to precipitation and other factors, we

213   chose to use a 3-month moving average to smooth the TWS residual (see Figure 2 (b)):

$$S[t] = f * S[t]_{\text{unsmoothed}} \tag{5}$$

214   where $*$ denotes the convolution operation, and f is the kernel [1/3, 1/3, 1/3] which is

215   convolved with the $S[t]_{\text{unsmoothed}}$ time series.

216   To address the inherent uncertainty, it becomes essential to employ a stochastic approach

217   that incorporates S along with its associated uncertainty. At each epoch, we postulate a

218   normal distribution with the mean being the obtained TWS residual $S[t]$ and $\sigma = \sigma_{S[t]}$.

219   Sampling from this distribution in each time step allows us to create realizations of the S

220   time series. Several methods exist for sampling from a Gaussian distribution, and one widely

221   used technique is the Box-Muller transform (Box & Muller, 1958). This method guarantees

222   generating a realization of S, which is independent epoch-wise with no artificial correlations.

223   We then use Monte Carlo Simulation (Mooney, 1997; Metropolis & Ulam, 1949) to generate
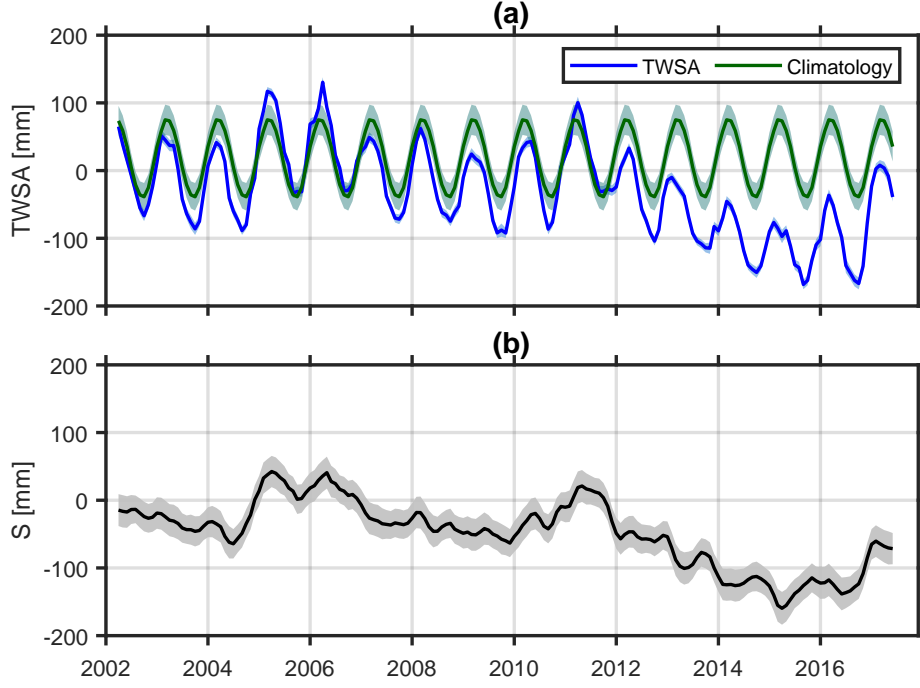
Figure 2. (a) Time series of the long-term TWSA from GRACE and the long-term climatology (1980–2012) from the hindcasted TWSA together with their uncertainties. At each epoch, we assume a Gaussian distribution for the uncertainties and the depicted uncertainty corresponds to the 1-σ level. Here the results are shown for the Death Valley basin in the US.

multiple realizations of S. Figure 3 shows 10 000 realization of TWS residual considering the 3-σ uncertainty. The density of the realizations is highest around the mean signal and decays following a Gaussian distribution. The colored lines overlaid on the time series depict the distribution of outcomes for three specific epochs: July 2004, May 2013, and April 2015.

To characterize drought within each time epoch, one common approach is to use the percentile rank method and the U.S. Drought Monitor (USDM) criteria. To this end, a set of five drought categories is defined (Table 1).

The quantile values for the S time series can be extracted as the inverse of the Cumulative Distribution Function (CDF), also known as the quantile function:

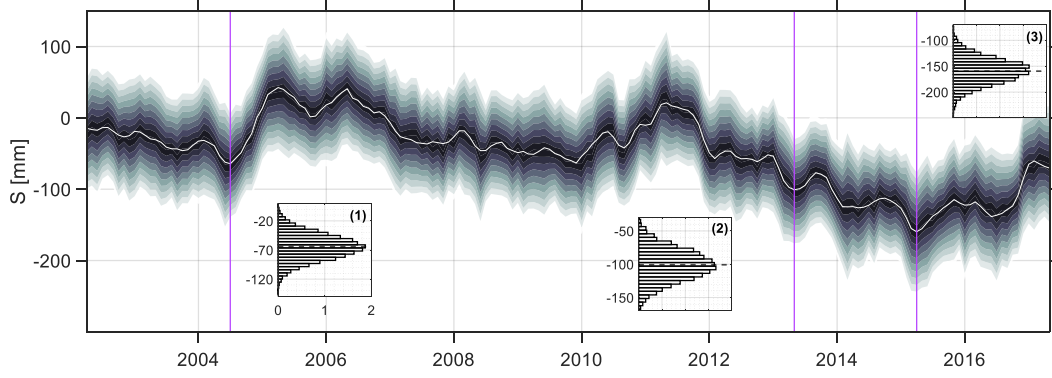$$Q(p) = F^{-1}(p) \tag{6}$$

Figure 3. The TWS residual (S) together with its 10 000 realizations, calculated using Monte Carlo simulation. Here the results are shown for the Death Valley basin in the US. The distribution of realizations for three epochs, namely July 2004, May 2013, and April 2015 are marked with colored dots over the time series and are shown in sub-figures.

Table 1. Drought categories and corresponding percentile ranges as defined by the U.S. Drought Monitor (USDM).

Drought Category	Description	Percentile Range
D0	Abnormally dry	20–30%
D1	Moderate drought	10–20%
D2	Severe drought	5–10%
D3	Extreme drought	2–5%
D4	Exceptional drought	Less than 2%

where $Q(p)$ represents the quantile function and $F^{-1}(p)$ denotes the inverse CDF evaluated at probability p. In a conventional deterministic approach, the drought category for each epoch is determined based on its quantile value of S. For example in Figure 4 (a), the dark solid line represents the quantile function of the S time series. Using such a function one can characterize drought for case (1), case (2), and case (3) as D4, D1, and no drought, respectively.

Such an approach overlooks the uncertainty in TWS residual S. However, accounting for uncertainty would entail obtaining the quantile function for all realizations of S. These functions form a cloud of points rather than a single line as it has been illustrated in Figure 4 (a). The quantile functions are shown in grayscale representing the probability $\Pr(p, S)$ for a given percentile p and TWS residual S. Already at this stage, a glance at Figure 4 (a) reveals the complexity introduced by the uncertainty envelope, challenging the conventional

245 approach to assigning a specific class to a particular measurement. It is noteworthy that the

246 uncertainty envelope depicted in Figure 4 (a) exhibits a stationarity character, indicating

247 general uncertainty in the data regardless of the specific time of measurements. This char-

248 acteristic is reflective of the general uncertainty of S, emphasizing the broader statistical

249 context rather than being tied to specific instances in time.

250 Now, let's delve into the characterization of drought for one of the measurements illustrated

251 in Figure 3. In this context, alongside the consideration of the stationary uncertainty as re-

252 flected in the quantile envelope and represented by $\Pr(p, S)$, it becomes essential to account

253 for the uncertainty associated with the measurement at that specific epoch. This is funda-

254 mentally crucial because two GRACE measurements with the same value of S may exhibit

255 varying levels of uncertainty. Therefore, we incorporate the probability density function of

256 the value S_t, denoted by $f(S_t)$, obtained from the mean and uncertainty of that epoch.

257 $f(S_t)$ is shown for the three sample epochs on the top right panel of Figure 4. At each

258 epoch, we multiply this probability density function with the entire distribution $\Pr(p, S)$,

259 as illustrated in Figure 4 (c). Essentially, this multiplication results in a down-weighting of

260 probabilities located in the tails of $f(S_t)$.

261 Once $\Pr(p, S) f(S_t)$ is achieved, to obtain PSDI at each epoch and for each drought category

262 D_i, we can integrate the probabilities both in S and p domains and normalize it with the

263 integral over the entire domain:

$$\text{PSDI}(t, D_i) = \frac{\int_S \int_{D_i} \Pr(p, S) f(S_t) \, dp \, ds}{\int_S \int_0^1 \Pr(p, S) f(S_t) \, dp \, ds} \tag{7}$$

264 By performing this process for all drought categories and time epochs, we generate a com-

265 prehensive probabilistic representation of drought severity over time. For decision-making

266 purposes, the highest-probability category can be judiciously chosen as the definitive drought

267 classification for a particular month. The flowchart of the proposed probabilistic approach
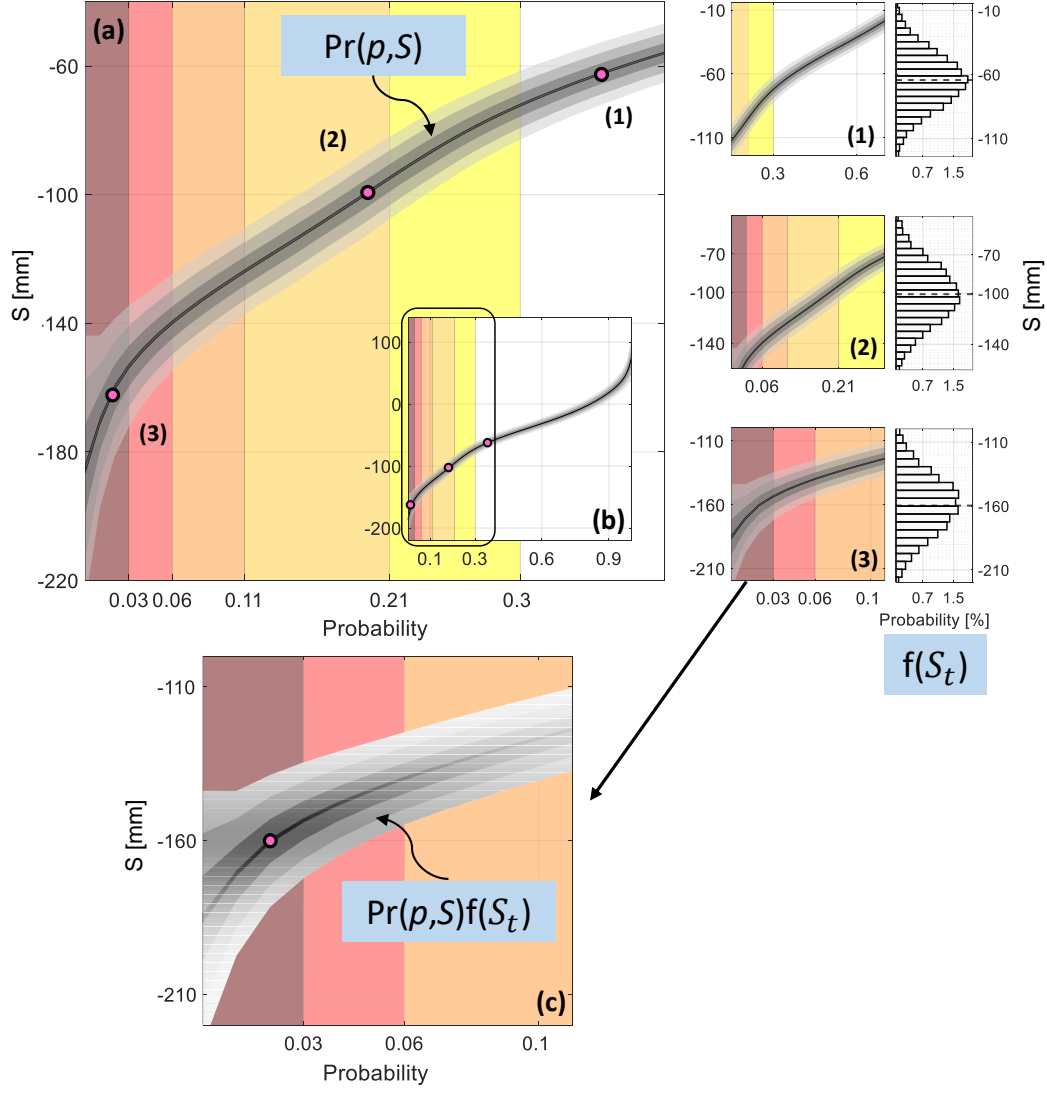
268 is shown in Figure 5.

Figure 4. (a) The quantile functions (inverse of the Cumulative Distribution Function (CDF)) of the S realizations are depicted. The varying shades of gray signify the density of data points, with darker shades indicating higher density. The drought categories, ranging from D0 to D4, are delineated within their respective percentile ranges, each denoted by its corresponding color. Colored dots illustrate the positions of the three cases from Figure 3 on the quantile functions plot. These cases are further elaborated in a magnified view, accompanied by the corresponding probability distribution derived from S and its associated uncertainty. (b) Similarly, as in (a), this visualization portrays the quantile functions plot, but encompasses the complete range of quantile values. (c) The density of the counted points after integrating the probability distribution stemming from the S and its corresponding uncertainty. It's important to note that the presented results are centered on the Death Valley basin within the United States.
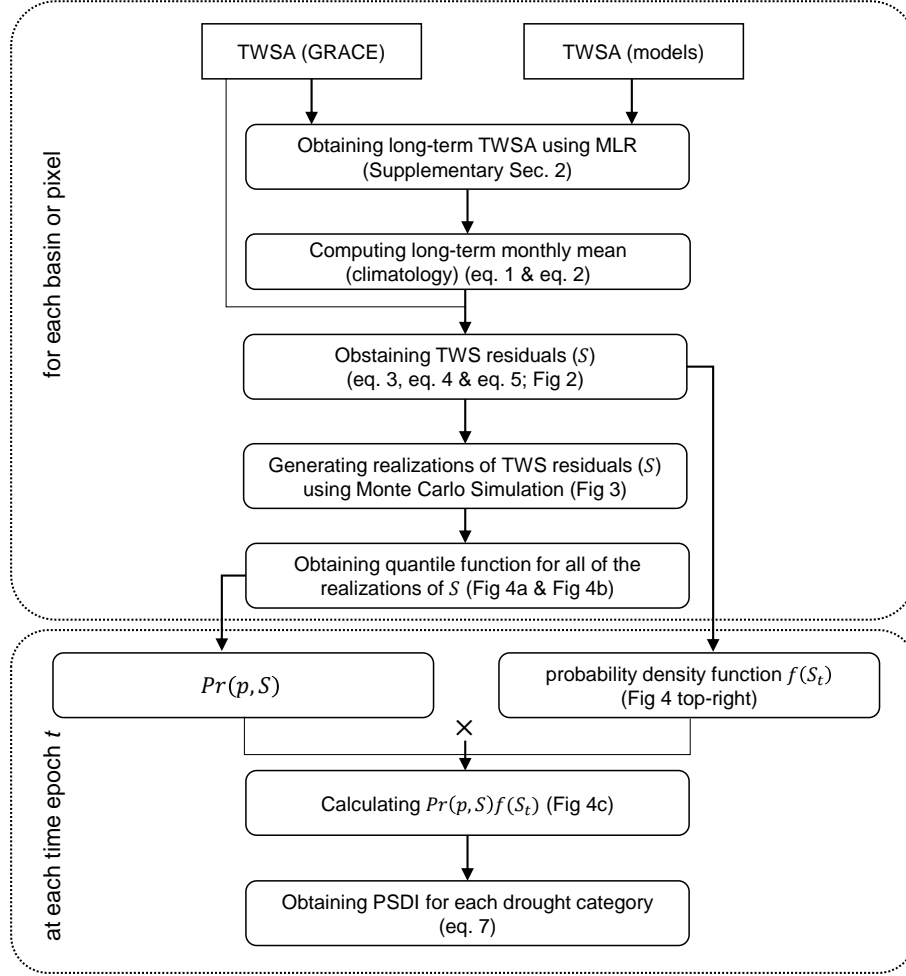
Figure 5. Flowchart of the proposed PSDI framework.

3 Results and Discussion

3.1 PSDI vs SDI

The PSDI approach offers a more nuanced understanding of drought conditions compared to the SDI approach. This is because PSDI captures the uncertainty associated with drought severity, while the SDI approach may oversimplify the classification of drought conditions. Although the SDI categorization is often the most probable category according to the PSDI, the neighboring categories may also have significant probabilities. This tendency becomes more pronounced as the intensity of the drought increases. This can be attributed to the

lower slope of the CDF curve over more severe droughts and the wider range of quantile values.

To delve deeper into the analysis, we have quantified the disparities between drought categorizations as defined by SDI and $PSDI_{max}$—the category of drought with the highest probability in PSDI—across the world's major river basins, with the exclusion of Greenland and Antarctica. The findings, illustrated in Figure 6 (a), shed light on the prevalence of these discrepancies throughout the study period spanning from 2003 to 2016. The ratio exhibits a range of variations, hovering near zero for basins such as Lake Balkhash in southeastern Kazakhstan or Po in Italy to a significant value of 30 % over Highland of Ethiopia and Somalia in Africa or Sao Francisco in Brazil. In general, the risk of mischaracterizing storage-based drought through the deterministic approach is notably high (exceeding 10 % in Figure 6 (a)) across Africa (excluding the northern region), Eastern Europe, Mongolia, Russia, and within the river basins of Nelson river, St. Lawrence, and Colorado (Argentina). In instances where discrepancies arise between SDI and $PSDI_{max}$, a predominant tendency is for SDI to overestimate the drought category. This is evident when comparing Figure 6 (b) and Figure 6 (c).

To investigate further, Figure 7 provides a visual comparison between two approaches for characterizing drought: probabilistic (PSDI) and deterministic (SDI), over several selected basins. The distribution of the basins is shown in the top panel of the Figure 7. For each basin, the drought categories, ranging from the status of no drought to exceptional drought (D4), are displayed in columns. The probability assigned to each category at every time step is depicted using gray scale. The deterministic perspective is illustrated with red boxes, allowing for a direct comparison of the two approaches.

The Danube and Ganges basins exhibited no disparity between SDI and $PSDI_{max}$ from 2015 to 2016. In contrast, the Mississippi basin displayed the most substantial mismatch between SDI and $PSDI_{max}$. It's noteworthy that these mismatches were confined to adjacent categories. Specifically, when considering mismatches spanning more than one category, only
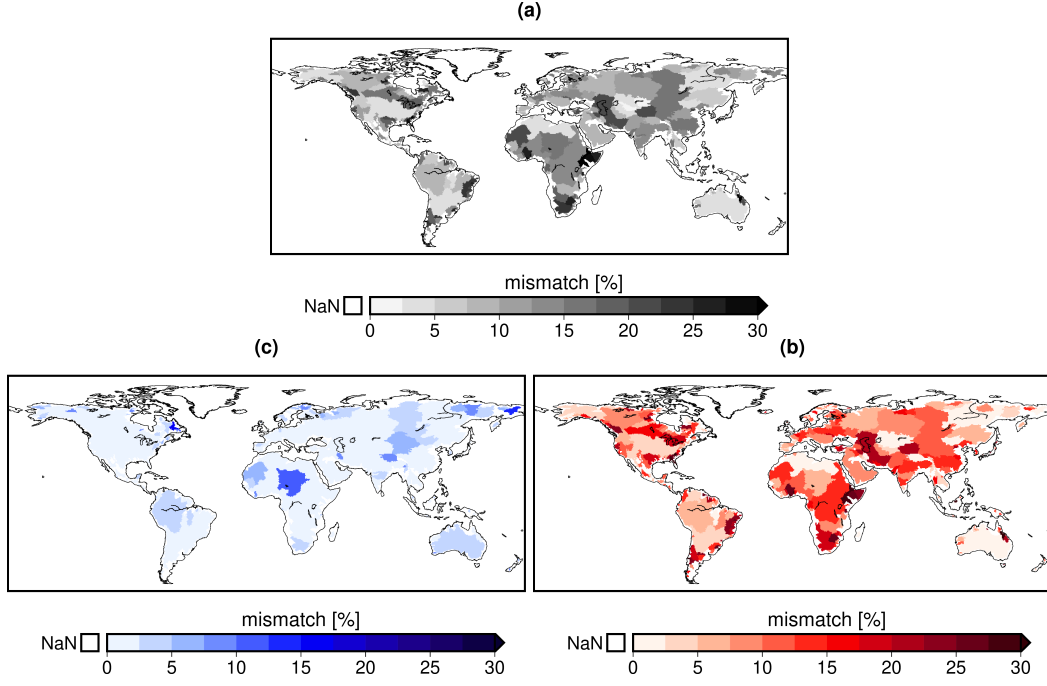
(a)

(c)   **(b)**

Figure 6. (a) Basin-wise distribution of the discrepancies between SDI and $PSDI_{max}$. The values represent the percentage of epochs where $PSDI_{max}$ differs from SDI by at least two drought categories. (b) the percentage of epochs with a discrepancy of more than one category higher in SDI compared to $PSDI_{max}$. (b) the percentage of epochs with a discrepancy of more than one category lower in SDI compared to $PSDI_{max}$. Greenland and Antarctica are excluded from the maps.

304 four basins had such occurrences: one month in Amazonas and Nile, two months in Niger,

305 and five months in Murray Darling. Across all basins, when a discrepancy arose between

306 SDI and $PSDI_{max}$, the SDI category consistently indicated a higher severity of drought.

Figure 7. Top: The global distribution of the selected basins. Bottom: The SDI (red boxes) together with PSDI (gray scale probability range) for selected basins. The basins are shown in two groups considering the period with more frequency of drought, the first row between 2015–2016 and the second row between 2006–2007. The "-" represents "no drought" or "normal state" of the water storage.

307   We have investigated further the sensitivity of different categories of drought to incorpo-

308 rating uncertainties into drought characterization. Figure 8 (a) visualizes the percentage

309 of epochs where PSDI_{max} differs from SDI by at least two drought categories. The results

310 suggest that such discrepancies can diverge significantly in the categorization of drought con-

311 ditions, especially in the D1, D2, and D3 categories, especially in D2. We have also compared

312 the ratio of the mismatch period with respect to different climate categories (Figure 8 (b)).

313 For more detailed information about the categories and the method of classification, please

314 see section 4 in the supplementary file. Although the mismatch range can vary from arid to

315 humid climate, the average value of the mismatch is the same over different climate regions,

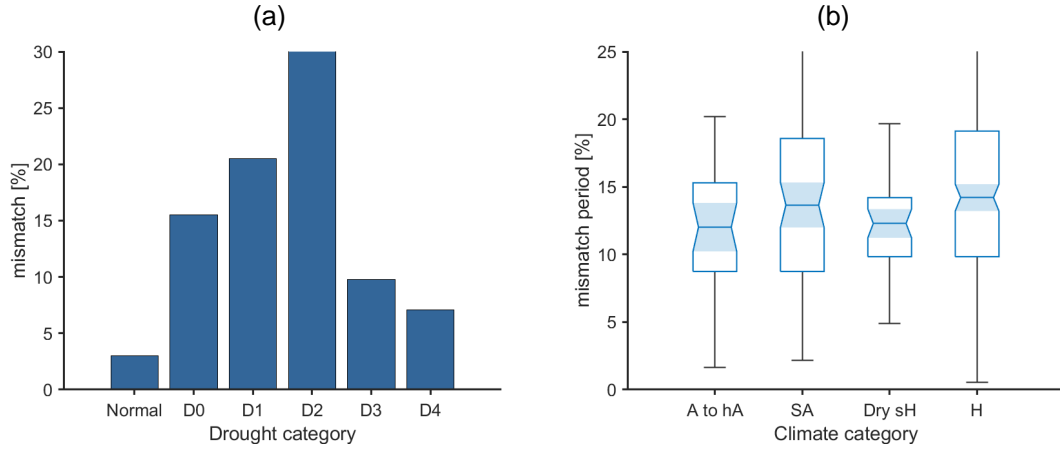316 with a slightly higher value for the Dry sub-humid regions (Dry sH).

Figure 8. (a) A barplot illustrates the percentage of epochs where PSDI_{max} diverges from SDI by at least two drought categories. (b) Boxplot of the mismatch between the PSDI_{max} and SDI over different climate categories, namely, arid to hyper-arid (A to hA), semi-arid (SA), dry sub-humid (Dry sH), and humid (H). It is noteworthy that to count the number of months, we have considered those with more than one category difference between the PSDI_{max} and SDI.

3.2 Performance of the PSDI during extreme hydrologic events

318 To assess the PSDI's reliability, we analyzed its performance during several well-documented

319 extreme hydrologic events between 2002 and 2016. The drought events during 2012 included

320 the moderate to exceptional drought over the United state (Boyer et al., 2013; Ault et al.,

321 2013), southern Europe (Oikonomou et al., 2020; Spinoni et al., 2015). The drought affected

many Middle East regions between 2007 and 2008 (Barlow et al., 2016). Southern Africa suffered from a severe to exceptional drought between 2005 and early 2006 (Nicholson, 2014), while central Argentina and Paraguay were affected by drought throughout 2009 (Guha-Sapir et al., 2016). Moreover, Australia experienced the worst drought recorded since European settlement in the 2000s, called the *Millennium drought*, with a peak in 2006 that affected many regions of the south to the east, including agricultural lands of the Murray-Darling basin (Van Dijk et al., 2013; Heberger, 2012). Figure 9 illustrates the performance of the PSDI over the events mentioned above. For each region, the category with the maximum probability and the estimated probability is shown for the selected date. Generally, the PSDI shows high performance in characterizing drought in the selected drought events (Figure 9). Comparing the SDI with $PSDI_{max}$ reveals that SDI categorizes higher drought intensities.
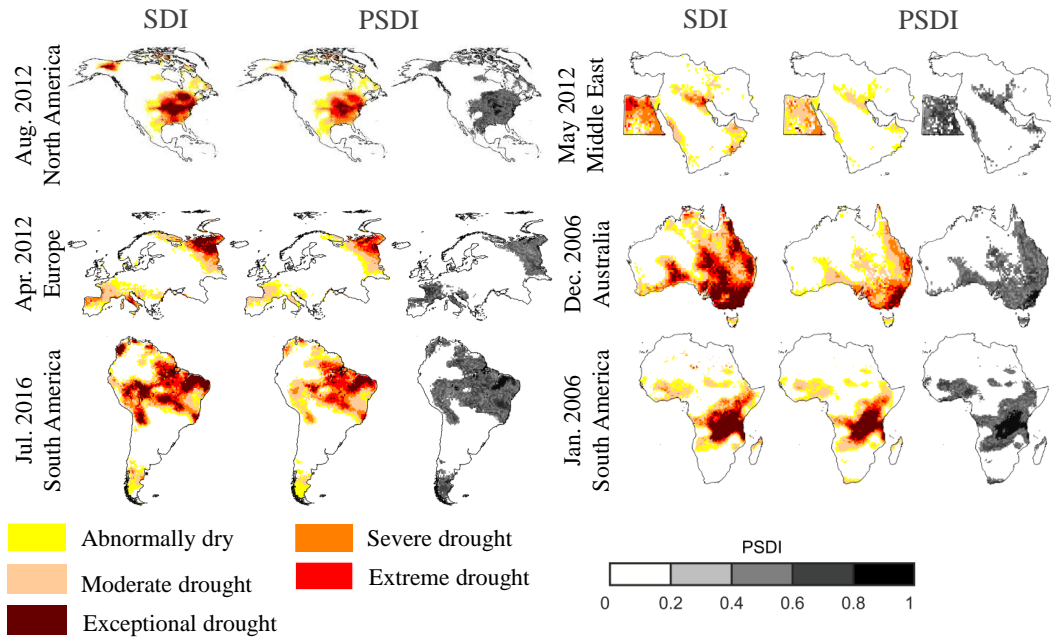

Figure 9. Comparing SDI with PSDI during some reported drought events.

4 Conclusions

For the first time, this study presents a probabilistic approach to characterizing TWS drought using time-variable gravity from satellite gravimetry. Our proposed framework acknowledges and addresses the inherent uncertainties associated with GRACE data. Our approach leverages Monte Carlo simulations to generate realistic realizations, capturing the stochastic nature of the TWSA time series. This ensemble reflects the diverse possible scenarios and their associated uncertainties, paving the way for a more insightful understanding of drought conditions. We have monitored the results of the proposed PSDI over major river basins and compared the result with SDI (deterministic approach). Our spatial analysis underscores the significance of adopting a probabilistic approach. It becomes evident that deterministic methodologies, in certain regions, tend to overestimate the severity of storage-based drought, potentially leading to misleading conclusions. While deterministic indices may tend to oversimplify drought categorization, PSDI accounts for uncertainty, thereby offering a more accurate representation of drought severity, particularly during extreme events.

Furthermore, our study assesses the performance of PSDI during well-documented extreme hydrologic events, spanning from the United States to Europe, the Middle East, Southern Africa, South America, and Australia. In each case, PSDI demonstrates its robustness in characterizing drought conditions. Comparing the SDI with $PSDI_{max}$ reveals that the drought can be categorized with more intensity using SDI with respect to the PSDI. We also address the uncertainties associated with different GRACE mascon products, emphasizing the importance of selecting the appropriate data source for reliable drought characterization. Variations in uncertainty estimates among different centers and processing methods highlight the need for caution when utilizing GRACE-derived data for drought analysis. We also shed light on the formal errors associated with GRACE data, highlighting the overestimation and underestimation tendencies of various solutions. This insight serves as a valuable

reference for researchers and institutions relying on GRACE data for drought monitoring and assessment.

The findings of this study underscore the importance of a probabilistic approach in characterizing drought over various regions and during several drought events. The new approach provides a more realistic characterization of drought by accounting for the uncertainties in the GRACE(-FO) TWSA data in contrast to the common deterministic approach. By embracing uncertainty and providing a comprehensive ensemble of drought scenarios, PSDI advances the field of drought assessment, offering improved accuracy and insight for decision-makers and researchers alike. In an era marked by changing climate patterns and increasing water stress, our probabilistic approach represents a significant step toward more effective drought management and adaptation strategies.

Author Contribution Statement

Peyman Saemian and Mohammad J. Tourian developed the method, conducted the data analysis, and wrote the paper. Omid Elmi contributed to the analysis and assisted in producing graphics. Amir Aghakouchak and Nico Sneeuw supported the study with discussions on algorithm development. All authors commented on and reviewed the manuscript, and contributed to the final version.

Open Research

In this study, we employed a diverse set of datasets. The GRACE data, the GSFC mascon product, is available at `https://earth.gsfc.nasa.gov/geo/data/grace-mascons`. Nine global water resources datasets, including PCR-GLOBWB, SURFEX-TRIP, HBV-SIMREG, HTESSEL, JULES, LISFLOOD, ORCHIDEE, SWBM, and W3RA, were obtained from the eartH2Observe Water Cycle Integrator (`ftp://wci.earth2observe.eu`). CLM5 products are accessible via Earth System Grid (Oleson et al., 2019). The WaterGAP Global Hydrology Model (WaterGAP v2.2d) data is accessible at `https://doi.pangaea`

`.de/10.1594/PANGAEA.918447`. Additionally, the fifth generation ECMWF atmospheric reanalysis (ERA5) data can be downloaded from the Copernicus Climate Change Service (C3S) at ECMWF (`https://cds.climate.copernicus.eu`). For the long-term TWSA from the MLR approach, the data is available in mat format at DaRUS "Data for: A probabilistic approach to characterizing drought using satellite gravimetry", `https://doi.org/10.18419/darus-3832`.

Acknowledgments

References

AghaKouchak, A., Farahmand, A., Melton, F., Teixeira, J., Anderson, M., Wardlow, B., & Hain, C. (2015). Remote sensing of drought: progress, challenges and opportunities. *Reviews of Geophysics*, *53*(2), 452–480. (doi: 10.1002/2014RG000456)

AghaKouchak, A., Huning, L. S., Sadegh, M., Qin, Y., Markonis, Y., Vahedifard, F., . . . others (2023). Toward impact-based monitoring of drought and its cascading hazards. *Nature Reviews Earth & Environment*, 1–14.

AghaKouchak, A., Mirchi, A., Madani, K., Di Baldassarre, G., Nazemi, A., Alborzi, A., . . .

others (2021). *Anthropogenic Drought: Definition, Challenges, and Opportunities.* Wiley Online Library. doi: 10.1029/2019RG000683

Ahmadalipour, A., Moradkhani, H., Yan, H., & Zarekarizi, M. (2017). Remote sensing of drought: vegetation, soil moisture, and data assimilation. In *Remote sensing of hydrological extremes* (pp. 121–149). Springer.

Ault, T., Henebry, G., De Beurs, K., Schwartz, M., Betancourt, J. L., & Moore, D. (2013). The false spring of 2012, earliest in North American record. *Eos, Transactions American Geophysical Union*, *94*(20), 181–182. doi: 10.1002/2013EO200001

Barlow, M., Zaitchik, B., Paz, S., Black, E., Evans, J., & Hoell, A. (2016). A review of drought in the Middle East and southwest Asia. *Journal of climate*, *29*(23), 8547–8574. doi: 10.1175/JCLI-D-13-00692.1

Behling, R., Roessner, S., Foerster, S., Saemian, P., Tourian, M. J., Portele, T. C., & Lorenz, C. (2022). Interrelations of vegetation growth and water scarcity in Iran revealed by satellite time series. *Scientific Reports*, *12*(1), 20784. doi: 10.1038/s41598-022-24712-6

Box, G. E., & Muller, M. E. (1958). A note on the generation of random normal deviates. *The annals of mathematical statistics*, *29*(2), 610–611. doi: 10.1214/aoms/1177706645

Boyer, J., Byrne, P., Cassman, K., Cooper, M., Delmer, D., Greene, T., . . . others (2013). The US drought of 2012 in perspective: a call to action. *Global Food Security*, *2*(3), 139–143. doi: 10.1016/j.gfs.2013.08.002

Coelho, C. A., & Goddard, L. (2009). El niño–induced tropical droughts in climate change projections. *Journal of Climate*, *22*(23), 6456–6476. doi: 10.1175/2009JCLI3185.1

Coumou, D., & Rahmstorf, S. (2012). A decade of weather extremes. *Nature climate change*, *2*(7), 491. doi: 10.1038/nclimate1452

Donat, M. G., Lowry, A. L., Alexander, L. V., O'Gorman, P. A., & Maher, N. (2016). More extreme precipitation in the world's dry and wet regions. *Nature Climate Change*, *6*(5), 508. doi: 10.1038/nclimate2941

Famiglietti, J. S., Lo, M., Ho, S. L., Bethune, J., Anderson, K., Syed, T. H., . . . Rodell, M. (2011). Satellites measure recent rates of groundwater depletion in California's Central

Valley. *Geophysical Research Letters*, *38*(3). doi: 10.1029/2010GL046442

FAO. (2021). Drought [Computer software manual]. (`http://www.fao.org/land-water/water/drought/en/`)

Gardner, A. S., Moholdt, G., Cogley, J. G., Wouters, B., Arendt, A. A., Wahr, J., . . . others (2013). A reconciled estimate of glacier contributions to sea level rise: 2003 to 2009. *science*, *340*(6134), 852–857. doi: 10.1126/science.1234532

Gouweleeuw, B. T., Kvas, A., Gruber, C., Gain, A. K., Mayer-Gürr, T., Flechtner, F., & Güntner, A. (2018). Daily GRACE gravity field solutions track major flood events in the Ganges–Brahmaputra Delta. *Hydrology and Earth System Sciences*, *22*(5), 2867–2880. doi: 10.5194/hess-22-2867-2018

Guha-Sapir, D., Below, R., & Hoyois, P. (2016). EM-DAT: the CRED/OFDA international disaster database. *Université Catholique de Louvain*. Retrieved from `https://www.emdat.be/`

Heberger, M. (2012). Australia's millennium drought: Impacts and responses. In *The world's water* (pp. 97–125). Springer.

Heim Jr, R. R. (2002). A review of twentieth-century drought indices used in the united states. *Bulletin of the American Meteorological Society*, *83*(8), 1149–1166. doi: 10.1175/1520-0477-83.8.1149

Hisdal, H., Stahl, K., Tallaksen, L. M., & Demuth, S. (2001). Have streamflow droughts in Europe become more severe or frequent? *International Journal of Climatology*, *21*(3), 317–333. doi: 10.1002/joc.619

Hosseini-Moghari, S.-M., Araghinejad, S., Ebrahimi, K., Tang, Q., & AghaKouchak, A. (2020). Using GRACE satellite observations for separating meteorological variability from anthropogenic impacts on water availability. *Scientific Reports*, *10*(1), 15098. doi: 10.1038/s41598-020-71837-7

Hulme, M. (1992). A 1951–80 global land precipitation climatology for the evaluation of general circulation models. *Climate dynamics*, *7*, 57–72. doi: 10.1007/BF00209609

Jiang, D., Wang, J., Huang, Y., Zhou, K., Ding, X., & Fu, J. (2014). The review of GRACE

data applications in terrestrial hydrology monitoring. *Advances in Meteorology*, *2014*. doi: 10.1155/2014/725131

Jones, P. D., & Hulme, M. (1996). Calculating regional climatic time series for temperature and precipitation: methods and illustrations. *International Journal of Climatology: A Journal of the Royal Meteorological Society*, *16*(4), 361–377. doi: 10.1002/(SICI)1097 -0088(199604)16:4⟨361::AID-JOC53⟩3.0.CO;2-F

Kreibich, H., Van Loon, A. F., Schröter, K., Ward, P. J., Mazzoleni, M., Sairam, N., . . . others (2022). The challenge of unprecedented floods and droughts in risk management. *Nature*, *608*(7921), 80–86. doi: 10.1038/s41586-022-04917-5

Kvas, A., Behzadpour, S., Ellmer, M., Klinger, B., Strasser, S., Zehentner, N., & Mayer-Gürr, T. (2019). ITSG-Grace2018: Overview and evaluation of a new GRACE-only gravity field time series. *Journal of Geophysical Research: Solid Earth*, *124*(8), 9332–9344. doi: 10.1029/2019JB017415

Li, W., Pan, R., Jiang, Z., Chen, Y., Li, L., Luo, J.-J., . . . Yu, J. (2021). Future changes in the frequency of extreme droughts over China based on two large ensemble simulations. *Journal of Climate*, *34*(14), 6023–6035.

Lorenz, C., Kunstmann, H., Devaraju, B., Tourian, M. J., Sneeuw, N., & Riegger, J. (2014). Large-scale runoff from landmasses: a global assessment of the closure of the hydrological and atmospheric water balances. *Journal of Hydrometeorology*, *15*(6), 2111–2139. doi: 10.1175/JHM-D-13-0157.1

Metropolis, N., & Ulam, S. (1949). The Monte Carlo method. *Journal of the American statistical association*, *44*(247), 335–341.

Mishra, A. K., & Singh, V. P. (2010). A review of drought concepts. *Journal of hydrology*, *391*(1-2), 202–216.

Mishra, A. K., & Singh, V. P. (2011). Drought modeling–a review. *Journal of Hydrology*, *403*(1-2), 157–175.

Mooney, C. Z. (1997). *Monte Carlo simulation* (Vol. 116). Sage publications.

Narasimhan, B., & Srinivasan, R. (2005). Development and evaluation of Soil Mois-

ture Deficit Index (SMDI) and Evapotranspiration Deficit Index (ETDI) for agricultural drought monitoring. *Agricultural and Forest Meteorology*, *133*(1-4), 69–88. doi: 10.1016/j.agrformet.2005.07.012

Naumann, G., Cammalleri, C., Mentaschi, L., & Feyen, L. (2021). Increased economic drought impacts in Europe with anthropogenic warming. *Nature Climate Change*, *11*(6), 485–491. doi: 10.1038/s41558-021-01044-3

Nicholson, S. E. (2014). A detailed look at the recent drought situation in the Greater Horn of Africa. *Journal of Arid Environments*, *103*, 71–79. doi: 10.1016/j.jaridenv.2013.12.003

Oikonomou, P. D., Karavitis, C. A., Tsesmelis, D. E., Kolokytha, E., & Maia, R. (2020). Drought characteristics assessment in Europe over the Past 50 Years. *Water Resources Management*, *34*(15), 4757–4772. doi: 10.1007/s11269-020-02688-0

Oleson, K., Lawrence, D., Lombardozzi, D., & Wieder, D. (2019). *CLM land-only release.* (Accessed: 2021-05-30) doi: https://doi.org/10.5065/d6154fwh

Palmer, W. C. (1965). *Meteorological drought* (Vol. 30). US Department of Commerce, Weather Bureau.

Reager, J. T., & Famiglietti, J. S. (2009). Global terrestrial water storage capacity and flood potential using GRACE. *Geophysical research letters*, *36*(23). doi: 10.1029/2009GL040826

Rodell, M., Chen, J., Kato, H., Famiglietti, J. S., Nigro, J., & Wilson, C. R. (2007). Estimating groundwater storage changes in the Mississippi River basin (USA) using GRACE. *Hydrogeology Journal*, *15*(1), 159–166. doi: 0.1007/s10040-006-0103-7

Rodell, M., Velicogna, I., & Famiglietti, J. S. (2009). Satellite-based estimates of groundwater depletion in India. *Nature*, *460*(7258), 999–1002. doi: 10.1038/nature08238

Saemian, P., Elmi, O., Vishwakarma, B., Tourian, M., & Sneeuw, N. (2020). Analyzing the Lake Urmia restoration progress using ground-based and spaceborne observations. *Science of The Total Environment*, *739*, 139857. doi: 10.1016/j.scitotenv.2020.139857

Saemian, P., Tourian, M. J., AghaKouchak, A., Madani, K., & Sneeuw, N. (2022). How much water did Iran lose over the last two decades? *Journal of Hydrology: Regional*

Studies, *41*, 101095. doi: 10.1016/j.ejrh.2022.101095

Scholz, C. A., Johnson, T. C., Cohen, A. S., King, J. W., Peck, J. A., Overpeck, J. T., ... others (2007). East african megadroughts between 135 and 75 thousand years ago and bearing on early-modern human origins. *Proceedings of the National Academy of Sciences*, *104*(42), 16416–16421.

Shepherd, A., Ivins, E., Rignot, E., Smith, B., Van Den Broeke, M., Velicogna, I., ... others (2018). Mass balance of the Antarctic Ice Sheet from 1992 to 2017. *Nature*, *558*, 219–222. doi: 10.1038/s41586-018-0179-y

Sinha, D., Syed, T. H., Famiglietti, J. S., Reager, J. T., & Thomas, R. C. (2017). Characterizing drought in India using GRACE observations of terrestrial water storage deficit. *Journal of Hydrometeorology*, *18*(2), 381–396. doi: 10.1175/JHM-D-16-0047.1

Sohn, B., Yeh, S.-W., Schmetz, J., & Song, H.-J. (2013). Observational evidences of Walker circulation change over the last 30 years contrasting with GCM results. *Climate Dynamics*, *40*, 1721–1732. doi: 10.1007/s00382-012-1484-z

Spinoni, J., Naumann, G., Vogt, J. V., & Barbosa, P. (2015). The biggest drought events in Europe from 1950 to 2012. *Journal of Hydrology: Regional Studies*, *3*, 509–524. doi: 10.1016/j.ejrh.2015.01.001

Sun, A. Y., Scanlon, B. R., AghaKouchak, A., & Zhang, Z. (2017). Using GRACE satellite gravimetry for assessing large-scale hydrologic extremes. *Remote Sensing*, *9*(12), 1287. doi: 10.3390/rs9121287

Svoboda, M., Fuchs, B., et al. (2016). *Handbook of drought indicators and indices.* World Meteorological Organization Geneva, Switzerland.

Svoboda, M., Hayes, M., & Wood, D. (2012). *Standardized precipitation index: user guide* (Tech. Rep. No. NO. 1090).

Svoboda, M., LeComte, D., Hayes, M., Heim, R., Gleason, K., Angel, J., ... others (2002). The drought monitor. *Bulletin of the American Meteorological Society*, *83*(8), 1181–1190.

Tapley, B. D., Bettadpur, S., Watkins, M., & Reigber, C. (2004). The gravity recovery and climate experiment: Mission overview and early results. *Geophysical research letters*,

31 (9). doi: 10.1029/2004GL019920

Teuling, A. J. (2018). A hot future for european droughts. *Nature Climate Change*, *8* (5), 364–365.

Thomas, A. C., Reager, J. T., Famiglietti, J. S., & Rodell, M. (2014). A GRACE-based water storage deficit approach for hydrological drought characterization. *Geophysical Research Letters*, *41* (5), 1537–1545. doi: 10.1002/2014GL059323

Tourian, M., Reager, J., & Sneeuw, N. (2018). The total drainable water storage of the Amazon river basin: A first estimate using GRACE. *Water Resources Research*, *54* (5), 3290–3312. doi: 10.1029/2017WR021674

Tourian, M. J., Elmi, O., Shafaghi, Y., Behnia, S., Saemian, P., Schlesinger, R., & Sneeuw, N. (2022). Hydrosat: geometric quantities of the global water cycle from geodetic satellites. *Earth System Science Data*, *14* (5), 2463–2486.

Tourian, M. J., Saemian, P., Ferreira, V. G., Sneeuw, N., Frappart, F., & Papa, F. (2023). A copula-supported Bayesian framework for spatial downscaling of GRACE-derived terrestrial water storage flux. *Remote Sensing of Environment*, *295*, 113685. doi: 10.1016/j.rse.2023.113685

van den Broeke, M., Bamber, J., Ettema, J., Rignot, E., Schrama, E., van de Berg, W. J., . . . Wouters, B. (2009). Partitioning recent Greenland mass loss. *science*, *326* (5955), 984–986. doi: 10.1126/science.1178176

Van Dijk, A. I., Beck, H. E., Crosbie, R. S., de Jeu, R. A., Liu, Y. Y., Podger, G. M., . . . Viney, N. R. (2013). The Millennium Drought in southeast Australia (2001–2009): Natural and human causes and implications for water resources, ecosystems, economy, and society. *Water Resources Research*, *49* (2), 1040–1057. doi: 10.1002/wrcr.20123

Voss, K. A., Famiglietti, J. S., Lo, M., De Linage, C., Rodell, M., & Swenson, S. C. (2013). Groundwater depletion in the Middle East from GRACE with implications for trans-boundary water management in the Tigris-Euphrates-Western Iran region. *Water resources research*, *49* (2), 904–914. doi: 10.1002/wrcr.20078

Wilhite, D. A. (2000). Chapter 1 drought as a natural hazard: Concepts and definitions.

Drought Mitigation Center Faculty Publications.

Wilhite, D. A., Svoboda, M. D., & Hayes, M. J. (2007). Understanding the complex impacts of drought: A key to enhancing drought mitigation and preparedness. *Water resources management*, *21*(5), 763–774. doi: 10.1007/s11269-006-9076-5

Yi, H., & Wen, L. (2016). Satellite gravity measurement monitoring terrestrial water storage change and drought in the continental United States. *Scientific reports*, *6*, 19909. doi: 10.1038/srep19909

Yi, S., Saemian, P., Sneeuw, N., & Tourian, M. J. (2023). Estimating runoff from pan-Arctic drainage basins for 2002–2019 using an improved runoff-storage relationship. *Remote Sensing of Environment*, *298*, 113816. doi: 10.1016/j.rse.2023.113816

Yirdaw, S. Z., Snelgrove, K. R., & Agboma, C. O. (2008). GRACE satellite observations of terrestrial moisture changes for drought characterization in the Canadian Prairie. *Journal of Hydrology*, *356*(1-2), 84–92. doi: 10.1016/j.jhydrol.2008.04.004

Yu, M., Li, Q., Hayes, M. J., Svoboda, M. D., & Heim, R. R. (2014). Are droughts becoming more frequent or severe in China based on the standardized precipitation evapotranspiration index: 1951–2010? *International Journal of Climatology*, *34*(3), 545–558. doi: 10.1002/joc.3701

Zargar, A., Sadiq, R., Naser, B., & Khan, F. I. (2011). A review of drought indices. *Environmental Reviews*, *19*(NA), 333–349. doi: doi.org/10.1139/a11-013

Zhao, C., Brissette, F., Chen, J., & Martel, J.-L. (2020). Frequency change of future extreme summer meteorological and hydrological droughts over north america. *Journal of Hydrology*, *584*, 124316.

Zhao, M., Geruo, A., Velicogna, I., & Kimball, J. S. (2017). A global gridded dataset of GRACE drought severity index for 2002–14: Comparison with PDSI and SPEI and a case study of the Australia millennium drought. *Journal of Hydrometeorology*, *18*(8), 2117–2129. doi: 10.1175/JHM-D-16-0182.1

Zhong, Y., Hu, E., Wu, Y., An, Q., Wang, C., Bai, H., & Gao, W. (2023). Reconstructing a long-term water storage-based drought index in the yangtze river basin. *Science of The*

607   *Total Environment*, *883*, 163403.

608   Zscheischler, J., Westra, S., Van Den Hurk, B. J., Seneviratne, S. I., Ward, P. J., Pitman,

609   A., . . . others (2018). Future climate risk from compound events. *Nature Climate Change*,

610   *8*(6), 469–477. doi: 10.1038/s41558-018-0156-3